

Office of Naval Research
Contract Nonr-220(57)
NR-064-487

Technical Report No. 8

TRANSIENT EXCITATION OF AN ELASTIC HALF-SPACE
BY A POINT LOAD TRAVELING ON THE SURFACE

by

D. C. Gakenheimer and J. Miklowitz

Distribution of this Document is Unlimited.

Division of Engineering and Applied Science
CALIFORNIA INSTITUTE OF TECHNOLOGY
Pasadena, California

January 1969

Office of Naval Research
Contract Nonr-220(57)
NR-064-487

Technical Report No. 8

Transient Excitation of an Elastic Half-Space
by a Point Load Traveling on the Surface

by

D. C. Gakenheimer and J. Miklowitz

Reproduction in whole or in part is permitted for
any purpose of the United States Government.

Distribution of this document is unlimited.

Division of Engineering and Applied Science
California Institute of Technology
Pasadena, California

January 1969

ABSTRACT

The propagation of transient waves in a homogeneous, isotropic, linearly elastic half-space excited by a traveling normal point load is investigated. The load is suddenly applied and then it moves rectilinearly at a constant speed along the free surface. The displacements are derived for the interior of the half-space and for all load speeds. Wave front expansions are obtained from the exact solution, in addition to results pertaining to the steady-state displacement field. The limit case of zero load speed is considered, yielding new results for Lamb's point load problem.

1. INTRODUCTION

Ground motions excited by moving surface forces arise, for example, from nuclear blasts and from shock waves generated by supersonic aircraft, and they interact with structures causing extensive damage. A mathematical problem of fundamental importance in these applications is that of an elastic half-space whose surface is excited by a normal point load which is suddenly applied and which subsequently moves rectilinearly at a constant speed.

In recent years several solutions to this problem have been given for the surface of the half-space. First Payton [1][†] computed the transient surface displacements by using an elastodynamic reciprocal theorem. Then Lansing [2] rederived some of Payton's results by employing a Duhamel superposition integral. However, no transient solutions have been given for the interior of the half-space, which are

[†]Numbers in brackets designate References at end of paper.

of interest with regard to buried structures. Therefore, it was appropriate to seek the interior displacements here. The remaining contributions to this problem are the steady-state results given by Mandel and Avramesco [3] , Papadopoulos [4] , Grimes [5] , Eason [6] , and Lansing [2] .

Of further interest is the fact that a point load moving on the surface of a half-space generates a non-axisymmetric disturbance. Very few wave propagation problems of this type have been solved and no general solution techniques are available. Beyond the moving load cases cited above, mention is made of Chao's work [7] on the surface displacements due to a tangential surface point load. However, like the moving load cases, Chao's solution technique is restricted to the surface of the half-space, besides involving a separation of variables which is peculiar to his excitation. Further, Scott and Miklowitz [8] have given a general method for solving non-axisymmetric wave propagation problems involving plates, but their technique was found not to be appropriate for the problem considered here. On the other hand, the solution technique developed here is applicable to all points of the half-space and it is sufficiently general that it should contribute guidelines for analyzing other non-axisymmetric half-space problems.

After formulating the problem in Section 2, a formal solution is obtained in Section 3 by using the Laplace and double Fourier transforms. Then in Section 4 the inverse transforms are evaluated by a technique due originally to Cagniard [9] , but simplified by a transformation introduced by DeHoop [10] for problems in acoustics and later used by Mitra [11] for an elastic half-space problem. In this way each displacement for the interior of the half-space is reduced to a sum of single integrals and algebraic terms for all values of the load speed. Each contribution to the displacements is identified as a specific wave.

In particular, the integrals represent waves which emanate from the initial position of the load as if they were generated by a stationary point source, while the algebraic terms represent disturbances that trail behind the load and whose wave geometry depends on the speed of the load relative to the body wave speeds. In Section 5 this form of the solution is exploited to evaluate the displacements near the wave fronts. Then in Section 6 the limit case of zero load speed is considered, showing that the integrals become a solution of Lamb's point load problem. Finally, in Section 7 the algebraic terms are shown to form the steady-state displacement field when the load speed exceeds both of the body wave speeds.

2. FORMULATION OF THE PROBLEM

The subject half-space problem is depicted in Fig. 1 based on a cartesian coordinate system (x, y, z) . The plane surface of the half-space is $z = 0$, with $z > 0$ forming the interior. A concentrated, normal load of unit magnitude travels on the surface along the positive x -axis at a constant speed c . The load acquires its velocity instantaneously at the origin of the coordinates at time $t = 0$.

The half-space is a homogeneous, isotropic medium governed by the equations of the linear theory of elasticity. The equations of motion for the case of vanishing body forces can be taken as the wave equations

$$\nabla^2 \phi = \frac{1}{c_d^2} \frac{\partial^2 \phi}{\partial t^2}, \quad \nabla^2 \tilde{\psi} = \frac{1}{c_s^2} \frac{\partial^2 \tilde{\psi}}{\partial t^2} \quad (1)$$

(characters underscored by a tilde designate vectors), where ϕ and $\tilde{\psi}$,

known as the Lamé potentials, are related to the displacement vector \underline{u} by

$$\underline{u} = \nabla\phi + \nabla \times \underline{\psi} \quad (2)$$

and satisfy the divergence condition

$$\nabla \cdot \underline{\psi} = 0 \quad (3)$$

The constants c_d and c_s , defined by $c_d^2 = (\lambda + 2\mu)/\nu$ and $c_s^2 = \mu/\nu$, represent the dilatational and equivoluminal body wave speeds, respectively, where λ and μ are the Lamé constants and ν is the material density. The stresses τ_{ij} are related to the displacements by

$$\tau_{ij} = \lambda u_{k,k} \delta_{ij} + \mu(u_{i,j} + u_{j,i}) \quad (4)$$

where tensor notation is employed.

The boundary conditions at $z = 0$ take the form

$$\left. \begin{aligned} \tau_{zz}(x, y, 0, t) &= -\delta(y)\delta(x - ct) \\ \tau_{xz}(x, y, 0, t) &= \tau_{yz}(x, y, 0, t) = 0 \end{aligned} \right\} \quad (5)$$

where δ is the Dirac delta function. To represent quiescence at $t = 0$, the initial conditions appear as

$$\phi(x, y, z, 0) = \frac{\partial \phi(x, y, z, 0)}{\partial t} = \underline{\psi}(x, y, z, 0) = \frac{\partial \underline{\psi}(x, y, z, 0)}{\partial t} = 0 \quad (6)$$

Finally, the potentials ϕ and $\underline{\psi}$, and the space derivatives of the potentials, are required to vanish at infinity.

3. FORMAL SOLUTION

A solution of the wave equations (1) that satisfies the initial conditions (6) and the boundedness condition at infinity can be computed

by using the Laplace and double Fourier transforms to suppress the time parameter and the x, y space coordinates. Then satisfying the boundary conditions (5), using the displacement-potential relation (2), and inverting the Fourier transform give the Laplace transformed displacements as

$$\bar{u}_j(x, y, z, p) = \bar{u}_{jd}(x, y, z, p) + \bar{u}_{js}(x, y, z, p) \quad (7)$$

for $j = x, y, z$, where

$$\bar{u}_{j\alpha}(x, y, z, p) = \frac{1}{(2\pi)^2} \int_{-\infty}^{\infty} \int_{-\infty}^{\infty} F_{j\alpha}(k, v, p) e^{-n_{\alpha}z + i(kx + vy)} dk dv \quad (8)$$

for $\alpha = d, s$, in which

$$\left. \begin{aligned} F_{xd}(k, v, p) &= -ikn_o G, & F_{xs}(k, v, p) &= 2ikn_d n_s G \\ F_{yd}(k, v, p) &= -ivn_o G, & F_{ys}(k, v, p) &= 2ivn_d n_s G \\ F_{zd}(k, v, p) &= n_d n_o G, & F_{zs}(k, v, p) &= -2n_d(k^2 + v^2)G, \end{aligned} \right\} \quad (9)$$

$$G = \frac{1}{(p + ick)T}, \quad (10)$$

$$T = n_o^2 - 4n_s n_d(k^2 + v^2), \quad (11)$$

$$n_d = (k^2 + v^2 + k_d^2)^{\frac{1}{2}}, \quad n_s = (k^2 + v^2 + k_s^2)^{\frac{1}{2}}, \quad n_o = [k_s^2 + 2(k^2 + v^2)], \quad (12)$$

$$k_d = \frac{p}{c_d}, \quad k_s = \frac{p}{c_s}, \quad (13)$$

\bar{u}_j and u_j are Laplace transform pairs, p is the Laplace transform parameter, k and v are the Fourier transform parameters, and the square roots n_d and n_s are assigned the branch that has the positive,

real part. In this form \bar{u}_j is expressed as the sum of a dilatational contribution \bar{u}_{jd} and an equivoluminal contribution \bar{u}_{js} .

4. INVERSION

The Laplace transform is inverted by a technique due to Cagniard [9] , but modified for the present application. This technique consists of converting each $\bar{u}_{j\alpha}$ into the Laplace transform of a known function, and then inverting the Laplace transform by inspection. In the subsequent calculations p is assumed to be a real, positive number. For such values of p , Lerch's theorem (see Carslaw and Jaeger [12]) guarantees that if $u_{j\alpha}$ exists, it is unique.

To simplify the form of $\bar{u}_{j\alpha}$, the transformations

$$k = \frac{p}{c_d} \beta \quad , \quad v = \frac{p}{c_d} \sigma \quad (14)$$

and

$$\beta = q \cos \theta - w \sin \theta \quad , \quad \sigma = q \sin \theta + w \cos \theta \quad (15)$$

are substituted successively into (8), yielding

$$\bar{u}_{j\alpha}(r, \theta, z, p) = \frac{1}{2} \int_0^\infty \int_{-\infty}^\infty K_{j\alpha}(q, w, \theta) e^{-\frac{p}{c_d}(m_\alpha z - iqr)} dq dw, \quad (16)$$

where

$$K_{xd}(q, w, \theta) = -[iq \cos \theta (iq \cos \theta + \gamma) + w^2 \sin^2 \theta] m_o L \quad , \quad (17a)$$

$$K_{xs}(q, w, \theta) = 2[iq \cos \theta (iq \cos \theta + \gamma) + w^2 \sin^2 \theta] m_d m_s L \quad , \quad (17b)$$

$$K_{yd}(q, w, \theta) = -\sin \theta [iq (iq \cos \theta + \gamma) - w^2 \cos \theta] m_o L \quad , \quad (17c)$$

$$K_{ys}(q, w, \theta) = 2 \sin \theta [iq (iq \cos \theta + \gamma) - w^2 \cos \theta] m_d m_s L \quad , \quad (17d)$$

$$K_{zd}(q, w, \theta) = (iq \cos \theta + \gamma) m_o m_d L \quad , \quad (17e)$$

$$K_{zs}(q, w, \theta) = -2(iq \cos \theta + \gamma)(q^2 + w^2) m_d L \quad , \quad (17f)$$

$$L = \frac{1}{\pi^2 c \mu [(iq \cos \theta + \gamma)^2 + w^2 \sin^2 \theta] R} \quad , \quad (18)$$

$$R = m_o^2 - 4m_d m_s (q^2 + w^2) \quad , \quad (19)$$

$$m_d = (q^2 + w^2 + 1)^{\frac{1}{2}} \quad , \quad m_s = (q^2 + w^2 + \ell^2)^{\frac{1}{2}} \quad , \quad m_o = [\ell^2 + 2(q^2 + w^2)] \quad , \quad (20)$$

$$\ell = \frac{c_d}{c_s} \quad , \quad \gamma = \frac{c_d}{c} \quad , \quad (21)$$

and (r, θ, z) are the cylindrical coordinates shown in Fig. 1. The transformation in (15) was introduced by DeHoop [10] in order to simplify Cagniard's technique.

In view of the symmetry properties

$$\left. \begin{aligned} \bar{u}_{x\alpha}(r, \theta, z, p) &= \bar{u}_{x\alpha}(r, -\theta, z, p) \\ \bar{u}_{y\alpha}(r, \theta, z, p) &= -\bar{u}_{y\alpha}(r, -\theta, z, p) \\ \bar{u}_{z\alpha}(r, \theta, z, p) &= \bar{u}_{z\alpha}(r, -\theta, z, p) \end{aligned} \right\} \quad (22)$$

$\bar{u}_{j\alpha}$, and hence \bar{u}_j , are only inverted for $0 \leq \theta \leq \pi$. Since $u_{j\alpha}$ has different forms depending on the speed of the load relative to the body wave speeds, the inversion of each $\bar{u}_{j\alpha}$ is separated into three cases. In particular, the terms supersonic, transonic, and subsonic refer to the cases when the load speed is greater than the dilatational wave speed ($c > c_d$), between the dilatational and equivoluminal wave speeds ($c_d > c > c_s$), and less than the equivoluminal wave speed ($c < c_s$), respectively. In

the remainder of this section \bar{u}_{zd} and \bar{u}_{zs} are inverted for the interior of the half-space ($z > 0$) and for all load speeds ($0 \leq c < \infty$). Then u_{zd} and u_{zs} are combined to give u_z , and similar results are displayed for u_x and u_y .

Dilatational Contribution for Supersonic Load Motion

From (16)

$$\bar{u}_{zd}(\tilde{x}, p) = \frac{1}{2} \int_0^\infty \int_{-\infty}^\infty K_{zd}(q, w, \theta) e^{-\frac{p}{c_d}(m_d z - iqr)} dq dw, \quad (23)$$

where \tilde{x} is the position vector. \bar{u}_{zd} is converted into the Laplace transform of a known function by mapping $(1/c_d)(m_d z - iqr)$ into t through a contour integration in a complex q -plane. To this end, the singularities of the integrand of \bar{u}_{zd} are branch points at $q = Q_d^\pm$ and $q = Q_s^\pm$, and simple poles at $q = Q_c^\pm$ and $q = Q_R^\pm$, where

$$\left. \begin{aligned} Q_d^\pm &= \pm i(w^2 + 1)^{\frac{1}{2}} & , & & Q_s^\pm &= \pm i(w^2 + \ell^2)^{\frac{1}{2}} \\ Q_c^\pm &= \frac{\pm w \sin \theta + i\gamma}{\cos \theta} & , & & Q_R^\pm &= \pm i(w^2 + \gamma_R^2)^{\frac{1}{2}} \end{aligned} \right\} \quad (24)$$

The poles at $q = Q_R^\pm$ correspond to the zeros of the Rayleigh function R , where $\gamma_R = c_d/c_R$ and c_R is the Rayleigh surface wave speed. The roots of these singularities which lie in the upper-half of the q -plane are shown in Fig. 2.

By seeking a particular contour in the q -plane such that

$$t = \frac{1}{c_d}(m_d z - iqr) \quad (25)$$

one finds, upon solving for q , that

$$q = q_d^\pm = \frac{c_d}{2} \left[itr \pm z(t^2 - t_{wd}^2)^{\frac{1}{2}} \right] \quad (26)$$

for $t \geq t_{wd}$, where

$$t_{wd} = \frac{\rho}{c_d} (w^2 + 1)^{\frac{1}{2}}, \quad \rho = (r^2 + z^2)^{\frac{1}{2}}. \quad (27)$$

Equation (26) defines one branch of a hyperbola with vertex $q = i(w^2 + 1)^{\frac{1}{2}} r / \rho$ and asymptotes $\arg q = \pm r / z$. As shown in Fig. 2 by a solid line labeled with q_d^+ and q_d^- , this hyperbola is parametrically described by t as t varies from t_{wd} towards infinity. Since $r / \rho < 1$, the hyperbola does not intersect the branch cuts in the q -plane. The arcs C_I and C_{II} are introduced as shown in Fig. 2 to form a closed contour C , where $C = \text{Re } q\text{-axis} + C_I + q_d^+ + q_d^- + C_{II}$.

The poles at $q = Q_c^{\pm}$ lie inside C if, and only if,

$$\begin{aligned} (1) \quad & -\frac{\pi}{2} < \theta < \frac{\pi}{2} \quad (\text{or } x > 0) \\ (2) \quad & \frac{c_d t r}{\rho^2} > \frac{\gamma}{\cos \theta} \quad (\text{or } t > t_L, \text{ where } t_L = \frac{\rho^2}{c x}) \\ (3) \quad & w \tan \theta > \frac{z c_d}{\rho^2} (t^2 - t_{wd}^2)^{\frac{1}{2}} \end{aligned} \quad (28)$$

For fixed t and $z > 0$, $t = t_L$ defines the surface of a hemisphere with center $(x = ct/2, n = 0)$ and radius $ct/2$. Conditions (2) and (3) are equivalent to the condition $w^2 > w_{od}^2$, where $w_{od}^2 = (\rho^2 \gamma^2 - x^2) z^2 \cos^2 \theta / x^2 n^2$ and $n = (y^2 + z^2)^{\frac{1}{2}}$. To incorporate these conditions into the contour integration for \bar{u}_{zd} , the half-space is separated into three regions:

Region I: $x > 0$, $\frac{x}{\rho} > \frac{c_d}{c}$

The poles at $q = Q_c^\pm$ lie inside C for $w \in [0, \infty)$.

Region II: $x > 0$, $\frac{x}{\rho} < \frac{c_d}{c}$

The poles at $q = Q_c^\pm$ lie inside C for $w \in (w_{od}, \infty)$ and they lie outside C for $w \in [0, w_{od})$. (28)

Region III: $x < 0$

No poles lie inside C for $w \in [0, \infty)$.

For $x > 0$, the rays $x/\rho = c_d/c$ form the surface of a cone whose axis is the positive x -axis. This conical surface is shown in Fig. 3a along with the part of $t = t_L$ which is bounded by $x/\rho < c_d/c$, and Roman numerals which depict the location of these regions in the half-space (each Roman numeral lies between the rays that define the corresponding region). The next step is to invert \bar{u}_{zd} for each of these regions.

Region I. The Cauchy-Goursat theorem and residue theory applied to the integrand of \bar{u}_{zd} and C yield

$$\bar{u}_{zd}(x, p) = \bar{A}_{zd}(x, p) + \bar{B}_{zd}(x, p) \quad , \quad (30)$$

where

$$\bar{A}_{zd}(x, p) = \int_0^\infty \int_{t_{wd}}^\infty \operatorname{Re} \left[K_{zd}(q_d, w, \theta) \frac{dq_d}{dt} \right] e^{-pt} dt dw \quad (31)$$

and

$$\bar{B}_{zd}(x, p) = \operatorname{Re} \int_0^\infty \left[K_{zd}(q, w, \theta) e^{-\frac{p}{c_d}(m_d z - iqr)} \right] \bigg|_{q=Q_c^+} dw \quad , \quad (32)$$

in which

$$\hat{K}_{zd}(q, w, \theta) = \frac{\sec \theta}{\pi c_d R} m_d m_o \quad (33)$$

\bar{A}_{zd} is the contribution from q_d^\pm , where $q_d = q_d^+$, and \bar{B}_{zd} is the residue contribution from the poles at $q = Q_c^\pm$. The integrals that arise along C_I and C_{II} vanish as these contours recede to infinity.

By interchanging the order of integration in (31) and inverting the Laplace transform, one finds

$$A_{zd}(x, t) = H(t - t_d) \int_0^{T_d} \text{Re} \left[K_{zd}(q_d, w, \theta) \frac{dq_d}{dt} \right] dw, \quad (34)$$

where

$$T_d = \left(\frac{t^2}{t_d^2} - 1 \right)^{\frac{1}{2}}, \quad t_d = \frac{p}{c_d}, \quad (35)$$

and H is the Heaviside function. A_{zd} is a hemispherical, dilatational wave in that it represents the disturbance behind the wave front at $t = t_d$, where t_d is the arrival time of a hemispherical, dilatational wave. This wave emanates from the initial position of the load as shown[†] in Fig. 3a.

The inversion of \bar{B}_{zd} is also done by a Cagniard technique. The singularities in the integrand of \bar{B}_{zd} are shown in Fig. 4 with branch points at $w = S_d^\pm$ and $w = S_s^\pm$, and simple poles at $w = S_R^\pm$, where

$$\left. \begin{aligned} S_d^\pm &= -i\gamma \sin \theta \pm i(1 - \gamma^2)^{\frac{1}{2}} \cos \theta \\ S_s^\pm &= -i\gamma \sin \theta \pm i(\ell^2 - \gamma^2)^{\frac{1}{2}} \cos \theta \\ S_R^\pm &= -i\gamma \sin \theta \pm i(\gamma_R^2 - \gamma^2)^{\frac{1}{2}} \cos \theta \end{aligned} \right\} \quad (36)$$

In Fig. 4 the convention is adopted that S_α^\pm and s_α^\pm represent roots of the same function, but whose positions are $w = S_\alpha^\pm$ for $c > c_\alpha$ and $w = s_\alpha^\pm$ for $c < c_\alpha$, where $\alpha = d, s, R$. Here, since $c > c_d$, only the S_α^\pm

[†] Arrival times are designated in the text by t subscripted with lower case letters and wave fronts are shown in the figures by solid lines.

arise and the s_{α}^{\pm} are given later in the text. The poles at $w = S_R^{\pm}$ correspond to the roots of the Rayleigh function R in which $q = Q_c^+$.

The particular contour in the w -plane is given by

$$t = \frac{1}{c_d} (m_d z - iqr) \Big|_{q = Q_c^+}, \quad (37)$$

or solving for w

$$w = w_d^{\pm} = -i\gamma \sin \theta + \frac{\gamma \cos \theta}{n^2} (i\xi y \pm z\alpha_d) \quad (38)$$

for $t \geq t_{dc}$, where

$$t_{dc} = \frac{1}{c} \left[\left(\frac{c^2}{c_d^2} - 1 \right)^{\frac{1}{2}} n + x \right]$$

$$\alpha_d = \left[\xi^2 - \left(\frac{c^2}{c_d^2} - 1 \right) n^2 \right]^{\frac{1}{2}} \quad (39)$$

$$\xi = ct - x.$$

Equation (38) defines one branch of a hyperbola with vertex $w = -i\gamma \sin \theta + i(y/n)(1 - \gamma^2)^{\frac{1}{2}} \cos \theta$ and asymptotes $\arg w = \pm y/z$. In view of the limits of integration in (32), only the plus root of (38) is needed and $w_d = w_d^+$. As shown in Fig. 4 by the solid contour labeled for region I, the w_d part of the hyperbola is parametrically described by t as t varies from t_{dc} towards infinity. Since $x/\rho > c_d/c$ and $y/n < 1$, w_d intersects the imaginary w -axis below the branch point at $w = S_d^+$ and above the real w -axis. As shown in Fig. 3a, t_{dc} represents the arrival time of a conical, dilatational wave which trails behind the load.

The contours C_0 and C_I are introduced as shown in Fig. 4 to

form a closed contour which includes w_d and the real w -axis. Then the application of the Cauchy-Goursat theorem to the integrand of \bar{B}_{zd} and this closed contour produces, upon inverting the Laplace transform,

$$B_{zd}(\underline{x}, t) = \text{Re} \left[\hat{K}_{zd}(w_d, \theta) \frac{dw_d}{dt} \right] H(t - t_{dc}) , \quad (40)$$

where

$$\hat{K}_{zd}(w, \theta) = \hat{K}_{zd}(Q_c^+, w, \theta) . \quad (41)$$

The integral that arises along C_I vanishes as C_I recedes to infinity and the one along C_O vanishes because its real part is zero. Finally, B_{zd} represents a conical, dilatational wave trailing behind the load.

The sum of A_{zd} and B_{zd} gives u_{zd} for region I as

$$u_{zd}(\underline{x}, t) = H(t - t_d) \int_0^{T_d} \text{Re} \left[K_{zd}(q_d, w, \theta) \frac{dq_d}{dt} \right] dw + \text{Re} \left[\hat{K}_{zd}(w_d, \theta) \frac{dw_d}{dt} \right] H(t - t_{dc}) . \quad (42)$$

Region II. By noting the conditions for region II in (29) and completing the contour integration in the q -plane, one finds

$$\bar{A}_{zd}(\underline{x}, p) = \int_0^\infty P \int_{t_{wd}}^\infty \text{Re} \left[K_{zd}(q_d, w, \theta) \frac{dq_d}{dt} \right] e^{-pt} dt dw \quad (43)$$

and

$$\bar{B}_{zd}(\underline{x}, p) = \text{Re} \int_{w_{od}}^\infty \left[\hat{K}_{zd}(q, w, \theta) e^{-\frac{p}{c_d}(m_d z - iqr)} \right] \bigg|_{q=Q_c^+} dw , \quad (44)$$

where \bar{u}_{zd} is the sum of \bar{A}_{zd} and \bar{B}_{zd} . The letter P precedes an improper integral to imply that it is interpreted in the sense of a Cauchy principal value. Such an integral arises in \bar{A}_{zd} because the poles at

$q = Q_c^\pm$ coalesce on q_d^\pm at $t = t_L$ as $w \rightarrow w_{od}$. Beyond this, \bar{A}_{zd} is exactly the same as for region I, while \bar{B}_{zd} only differs in the lower limit, which is expected since the poles at $q = Q_c^\pm$ only lie inside C for $w > w_{od}$.

The inversion of \bar{B}_{zd} proceeds as for region I, but with modifications in the geometry of the w -plane. For region II the particular contour w_d intersects the real w -axis as shown in Fig. 4, to comply with the limits of integration in \bar{B}_{zd} . Furthermore, the singularities S_d^+ , S_s^+ , and S_R^+ may lie below the real w -axis, but still on the imaginary w -axis, in a manner which is not shown in Fig. 4. However, since the particular contour does not intersect the imaginary w -axis, this has no bearing on the contour integration for region II. Then inverting \bar{A}_{zd} and \bar{B}_{zd} , and combining the results give u_{zd} for region II as

$$u_{zd}(x, t) = H(t - t_d) P \int_0^{T_d} \text{Re} \left[K_{zd}(q_d, w, \theta) \frac{dq_d}{dt} \right] dw + \text{Re} \left[\hat{K}_{zd}(w_d, \theta) \frac{dw_d}{dt} \right] H(t - t_L) \quad (45)$$

The first term in u_{zd} represents a hemispherical, dilatational wave as for region I. However, for region II the integral is interpreted as a Cauchy principal value for $t = t_L$. The second term has the same algebraic form as for region I, but the conical wave front is replaced with the hemispherical surface $t = t_L$. This new surface is not expected to be a wave front (i.e., u_{zd} and all the derivatives of u_{zd} are expected to be continuous through $t = t_L$) because it is not a characteristic surface (similar to $t = t_d$), or the closure of characteristic surfaces (similar to $t = t_{dc}$), associated with the governing wave equation for the dilatational potential ϕ in (1).

Region III. As indicated in (29) for region III no poles lie inside C. Therefore, the inversion of \bar{u}_{zd} proceeds exactly as for region I, less the residue term \bar{B}_{zd} , and u_{zd} can be obtained from (42) by deleting the algebraic term.

Summary. By comparing the results for each region it follows that u_{zd} can be represented by one expression for all three regions; namely,

$$u_{zd}(x, t) = H(t - t_d) P \int_0^{T_d} \operatorname{Re} \left[K_{zd}(q_d, w, \theta) \frac{dq_d}{dt} \right] dw + \operatorname{Re} \left[\hat{K}_{zd}(w_d, \theta) \frac{dw_d}{dt} \right] H(t - t_{dc}) H(t - t_L) H(x) . \quad (46)$$

This expression is valid for $0 \leq \theta \leq \pi$ and $z > 0$. The wave pattern associated with u_{zd} is shown in Fig. 3a, where the relationship between the rays $x/\rho = c_d/c$, the wave fronts $t = t_d$ and $t = t_{dc}$, the hemispherical surface $t = t_L$, and the regions I-III is depicted.

Dilatational Contribution for Transonic and Subsonic Load Motion

The inversion of \bar{u}_{zd} for $c_s < c < c_d$ and $c < c_s$, or equivalently $c < c_d$, proceeds exactly as for $c > c_d$, except that of the three regions in (29) only II and III are applicable for $c < c_d$ because x/ρ is always less than c_d/c . These two regions are depicted in Fig. 3b by Roman numerals two and three.

The inversion of \bar{u}_{zd} for region II proceeds for $c < c_d$ as it did for $c > c_d$, except that the geometry of the w -plane is different. As shown in Fig. 4, the position of the singularities varies depending on the value of c relative to c_s , c_d , and c_R . In that figure

$$\left. \begin{aligned} g_d^{\pm} &= -i\gamma \sin \theta \pm (\gamma^2 - 1)^{\frac{1}{2}} \cos \theta \\ g_s^{\pm} &= -i\gamma \sin \theta \pm (\gamma^2 - \ell^2)^{\frac{1}{2}} \cos \theta \\ g_R^{\pm} &= -i\gamma \sin \theta \pm (\gamma^2 - \gamma_R^2)^{\frac{1}{2}} \cos \theta \end{aligned} \right\} \quad (47)$$

However, the particular contour in the w -plane for region II remains the same for all load speeds ($c > c_d$ and $c < c_d$), as does the result of a contour integration which includes it and the real w -axis. Therefore, u_{zd} for region II and $c < c_d$ is the same as given for $c > c_d$ in (45). Furthermore, the inversion of \bar{u}_{zd} for region III is independent of the value of the load speed (which only appears through the position of the poles at $q = Q_c^{\pm}$) and the result is the same as given for $c > c_d$. Then combining the results for regions II and III gives u_{zd} for $c < c_d$ as

$$\begin{aligned} u_{zd}(x, t) &= H(t - t_d) P \int_0^{T_d} \operatorname{Re} \left[K_{zd}(q_d, w, \theta) \frac{dq_d}{dt} \right] dw \\ &\quad + \operatorname{Re} \left[\hat{K}_{zd}(w_d, \theta) \frac{dw_d}{dt} \right] H(t - t_L) H(x) \quad , \end{aligned} \quad (48)$$

where $0 \leq \theta \leq \pi$ and $z > 0$. The dilatational wave pattern for $c < c_d$ is shown in Fig. 3b. As expected physically, the conical wave front does not exist, leaving only the hemispherical one.

Finally, by comparing (46) and (48) one finds that u_{zd} is given by (46) for all load speeds if the Heaviside function satisfies the condition

$$H(t - t_{dc}) = 1 \quad (49)$$

for $c < c_d$.

Equivoluminal Contribution

The inversion of \bar{u}_{zs} proceeds as for \bar{u}_{zd} , but u_{zs} is more complicated than u_{zd} due to the appearance of head waves (or von Schmit waves).

With \bar{u}_{zs} being given by (16) for $j = z$ and $\alpha = s$, the corresponding q -plane is shown in Fig. 2, where the singularities are the same as for \bar{u}_{zd} , but the particular contour has two possible configurations, which are denoted by dashed lines. If $r/\rho < c_s/c_d$ and $w \in [0, \infty)$ or if $r/\rho > c_s/c_d$ and $w \in (w_1, \infty)$, where $w_1 = (r^2 \ell^2 - \rho^2)^{1/2}/z$, then the particular contour is similar to q_d^\pm and it is denoted by q_s^\pm , where

$$q_s^\pm = \frac{c_d}{\rho} \left[i t r \pm z (t^2 - t_{ws}^2)^{\frac{1}{2}} \right] \quad (50)$$

for $t \geq t_{ws}$, in which

$$t_{ws} = \frac{\rho}{c_d} (w^2 + \ell^2)^{\frac{1}{2}}. \quad (51)$$

However, if $r/\rho > c_s/c_d$ and $w \in [0, w_1)$, then the vertex of q_s^\pm lies on the branch cut between the branch points at $q = Q_d^+$ and $q = Q_s^+$, and the particular contour is given by q_s^\pm plus q_{sd} , where

$$q_{sd} = \frac{i c_d}{\rho} \left[t r - z (t_{ws}^2 - t^2)^{\frac{1}{2}} \right] \quad (52)$$

for $t_{ws} \leq t \leq t_{wsd}$, in which

$$t_{wsd} = \frac{1}{c_d} \left[(\ell^2 - 1)^{\frac{1}{2}} z + (w^2 + 1)^{\frac{1}{2}} r \right]. \quad (53)$$

As shown in Fig. 2, the closed contour C now includes q_s^\pm , q_{sd} when it arises, and the real q -axis. As for \bar{u}_{zd} , the poles at $q = Q_c^\pm$ can lie

either inside or outside of C .

In regard to the various positions of the poles at $q = Q_c^\pm$ and the vertex of q_s^\pm , the inversion of \bar{u}_{zs} is separated into seven cases, each of which corresponds to a particular region of the half-space:

$$\text{Region I: } x > 0, \frac{x}{\rho} > \frac{c_s}{c}, \frac{r}{\rho} < \frac{c_s}{c_d}, \frac{x}{r} > \frac{c_d}{c}$$

The poles lie inside C for $w \in [0, \infty)$.

The vertex does not lie on the branch cut for $w \in [0, \infty)$.

$$\text{Region II: } x > 0, \frac{x}{\rho} > \frac{c_s}{c}, \frac{r}{\rho} > \frac{c_s}{c_d}, \frac{x}{r} > \frac{c_d}{c}$$

The poles lie inside C for $w \in [0, \infty)$.

The vertex lies on the branch cut for $w \in [0, w_1)$.

$$\text{Region III: } x > 0, \frac{x}{\rho} > \frac{c_s}{c}, \frac{r}{\rho} > \frac{c_s}{c_d}, \frac{x}{r} < \frac{c_d}{c}$$

The vertex lies on the branch cut for $w \in [0, w_1)$.

The poles lie inside C for $w \in (0, \infty)$ and coalesce on q_{sd} as $w \rightarrow 0$. The poles also coalesce on q_{sd} as $\theta \rightarrow 0$ for $c_s < c < c_d$ and $w \in [0, (\gamma^2 - 1)^{\frac{1}{2}})$.

$$\text{Region IV: } x > 0, \frac{x}{\rho} < \frac{c_s}{c}, \frac{r}{\rho} < \frac{c_s}{c_d}$$

The poles lie inside C for $w \in (w_{os}, \infty)$.

The vertex does not lie on the branch cut for $w \in [0, \infty)$.

$$\text{Region V: } x > 0, \frac{x}{\rho} < \frac{c_s}{c}, \frac{r}{\rho} > \frac{c_s}{c_d}$$

The poles lie inside C for $w \in (w_{os}, \infty)$.

The vertex lies on the branch cut for $w \in [0, w_1)$.

The poles coalesce on q_{sd} as $\theta \rightarrow 0$ for $c < c_d$ and $w \in (w_{os}, (\gamma^2 - 1)^{\frac{1}{2}})$.

Region VI: $x < 0$, $\frac{r}{\rho} < \frac{c_s}{c_d}$

No poles lie inside C for $w \in [0, \infty)$.

The vertex does not lie on the branch cut for $w \in [0, \infty)$.

Region VII: $x < 0$, $\frac{r}{\rho} > \frac{c_s}{c_d}$

No poles lie inside C for $w \in [0, \infty)$.

The vertex lies on the branch cut for $w \in [0, w_1)$.

(Regions I - VII are referred to in the text by (54))

In (54), $w_{os} = (\rho^2 \gamma^2 - x^2 \ell^2)^{\frac{1}{2}} z \cos \theta / x n$. For $x > 0$, the rays $x/\rho = c_s/c$ form the surface of a cone which is similar to $x/\rho = c_d/c$, and $x/r = c_d/c$ defines two planes, one for $\theta > 0$ and one for $\theta < 0$. Also, $r/\rho = c_s/c_d$ defines the surface of a cone whose axis is the positive z -axis. All seven regions arise when inverting \bar{u}_{zs} for $c > c_d$, but only regions III-VII and regions IV-VII arise for $c_s < c < c_d$ and $c < c_s$, respectively. The Roman numerals in Figs. 5 - 8 depict the location of these regions in the half-space.

By inverting \bar{u}_{zs} for each region, accounting for the variable load speed, and combining the results, one finds

$$\begin{aligned}
 u_{zs}(x, t) = & H(t-t_s) P \int_0^T \text{Re} \left[K_{zs}(q_s, w, \theta) \frac{dq_s}{dt} \right] dw \\
 & + H(t-t_{sd}) H(t_B - t) H\left(\frac{r}{\rho} - \frac{c_s}{c_d}\right) P \int_{A_{sd}}^{T_{sd}} \text{Re} \left[K_{zs}(q_{sd}, w, \theta) \frac{dq_{sd}}{dt} \right] dw \\
 & + \text{Re} \left[\hat{K}_{zs}(w_{sd}, \theta) \frac{dw_{sd}}{dt} \right] H(t-t_{sc}) H(t-t_L) H(x) \\
 & + \text{Re} \left[\hat{K}_{zs}(w_{sd}, \theta) \frac{dw_{sd}}{dt} \right] H\left(\frac{y}{n} - \phi_c\right) \left[H(t-t_{sdc}) H\left(\frac{x}{r} - \frac{c_d}{c}\right) \right. \\
 & \left. + H(t-t_E) H\left(\frac{x}{\rho} - \frac{c_s}{c}\right) H\left(\frac{c_d}{c} - \frac{x}{r}\right) - H(t-t_{sc}) H\left(\frac{x}{\rho} - \frac{c_s}{c}\right) \right] H(x) \quad (55)
 \end{aligned}$$

for $0 \leq \theta \leq \pi$, $z > 0$, and $0 \leq c < \infty$. Further details on inverting \bar{u}_{zs} are given in a thesis by the first author [13]. The symbols in u_{zs} which have not been previously defined are

$$\hat{K}_{zs}(w, \theta) = \frac{-2 \sec \theta}{\pi c \mu R} m_d(q^2 + w^2) \Big|_{q = Q_c^+}, \quad (56)$$

$$\left. \begin{aligned} w_s &= -i\gamma \sin \theta + \frac{\gamma \cos \theta}{n^2} (i\xi y + z\alpha_s) \\ w_{sd} &= -i\gamma \sin \theta + \frac{i\gamma \cos \theta}{n^2} (\xi y - z\alpha_{sd}) \end{aligned} \right\} \quad (57)$$

$$\alpha_s = \left[\xi^2 - \left(\frac{c^2}{c_s^2} - 1 \right) n^2 \right]^{\frac{1}{2}}, \quad \alpha_{sd} = \left[\left(\frac{c^2}{c_s^2} - 1 \right) n^2 - \xi^2 \right]^{\frac{1}{2}}, \quad (58)$$

$$A_{sd} = \begin{cases} 0 & \text{for } t < t_s \\ T_s & \text{for } t > t_s \end{cases}, \quad (59)$$

$$T_s = \left(\frac{t^2}{t_s^2} - 1 \right)^{\frac{1}{2}} \ell, \quad T_{sd} = \left[\left(\frac{c_d(t-t_{sd})}{r} + 1 \right)^2 - 1 \right]^{\frac{1}{2}}, \quad (60)$$

$$\left. \begin{aligned} t_s &= \frac{\rho}{c_s}, \quad t_{sd} = \frac{1}{c_d} \left[(\ell^2 - 1)^{\frac{1}{2}} z + r \right], \\ t_B &= \frac{\rho^2 (\ell^2 - 1)^{\frac{1}{2}}}{z c_d}, \quad t_E = \frac{1}{c x} \left[\left(\frac{c^2}{c_s^2} x^2 - r^2 \right)^{\frac{1}{2}} z + r^2 \right] \\ t_{sc} &= \frac{1}{c} \left[\left(\frac{c^2}{c_s^2} - 1 \right)^{\frac{1}{2}} n + x \right], \quad t_{sdc} = \frac{1}{c} \left[\left(\frac{c^2}{c_s^2} - \frac{c^2}{c_d^2} \right)^{\frac{1}{2}} z + \left(\frac{c^2}{c_d^2} - 1 \right)^{\frac{1}{2}} y + x \right], \end{aligned} \right\} \quad (61)$$

$$\phi_c = \frac{\left(\frac{c^2}{c_d^2} - 1 \right)^{\frac{1}{2}}}{\left(\frac{c^2}{c_s^2} - 1 \right)^{\frac{1}{2}}}. \quad (62)$$

The Heaviside function in (55) is restricted by the conditions

$$\left. \begin{aligned} H(t - t_{sc}) &= 1 \quad \text{if } c < c_s \\ H(\frac{Y}{n} - \phi_c) &= 1 \quad \text{if } c < c_d \end{aligned} \right\} \quad (63)$$

The wave geometry associated with u_{zs} is shown in Figs. 5 - 9. The dilatational wave fronts are included in these diagrams for reference; therefore, they display the wave geometry associated with the total displacement u_z . However, the Roman numerals in these diagrams only correspond to u_{zs} and the regions described in (54).

The first and third terms in u_{zs} , which are analogous to the dilatational waves in u_{zd} , represent hemispherical and conical, equivoluminal waves, respectively. The second term in u_{zs} is the contribution from q_{sd} along the imaginary axis in the q -plane and it represents a head wave whose wave front is the surface of the truncated cone given by $t = t_{sd}$ for $r/\rho > c_s/c_d$. This wave, referred to as the conical head wave, is generated by the surface intersection of the dilatational wave front at $t = t_d$ and it propagates in front of $t = t_B$, as shown in Figs. 7 and 8(a,b); thereby, contributing both ahead and behind the equivoluminal wave front at $t = t_s$ for $r/\rho > c_s/c_d$. For fixed time, $t = t_B$ is the surface of a sphere with center $(r = 0, z = c_d t / 2(\ell^2 - 1)^{\frac{1}{2}})$ and radius $c_d t / 2(\ell^2 - 1)^{\frac{1}{2}}$. The surface $t = t_B$ is not expected to be a wave front because it is not a characteristic surface, or the closure of characteristic surfaces, of the wave equation for the equivoluminal potential ψ in (1).

The integral in the second term of u_{zs} is improper for $t = t_s$ because its integrand contains a first-order singularity at $w = 0$ (i.e., its integrand behaves like $1/w$ as $w \rightarrow 0$). This singularity is introduced by the differential of q_{sd} . In Section 5 this integral is evaluated

for $t \rightarrow t_s$, displaying a logarithmic singularity in u_{zs} for $t = t_s$. This integral is also improper for certain points in the plane under the path of the load (the $\theta = 0$ plane). In particular, it is interpreted as a Cauchy principal value for $t_{sc} < t < t_{sdc}^0$ if $\theta = 0$, $x/\rho > c_s/c$, and $c_s < c < c_d$; and for $t_L < t < t_{sdc}^0$ if $\theta = 0$, $x/\rho < c_s/c$, and $c < c_d$, where t_{sdc}^0 equals t_{sdc} evaluated for $\theta = 0$ and $t = t_{sdc}^0$ is shown in Fig. 8(a,b) by a dashed line projecting out from the load. The improper integral for $\theta = 0$ reflects the way the poles at $q = Q_c^\pm$ coalesce on q_{sd} as $\theta \rightarrow 0$, and as described in (54) for regions III and V. Furthermore, if the Cauchy principal value is evaluated for $\theta \rightarrow 0$, it combines with the remaining terms in u_{zs} to render u_{zs} continuous as $\theta \rightarrow 0$, which is expected physically.

The integral in the second term of u_{zs} is also improper for $t = t_E$ if $c > c_s$ and $x > 0$ because its integrand has a first-order singularity at $w = 0$ (note $t_E < t_s$, therefore $A_{sd} = 0$). This singularity reflects the way the poles at $q = Q_c^\pm$ coalesce on q_{sd} as $w \rightarrow 0$, and as described in (54) for region III. The significance of $t = t_E$ is discussed in connection with the last term in u_{zs} .

The last term in u_{zs} represents another head wave. This term is the contribution from the contour w_{sd} which is indicated in Fig. 4 as a segment of the imaginary w -axis. The dashed contour that is shown in this figure along with w_{sd} is the particular contour which arises in the w -plane for \bar{u}_{zs} and region II if $y/n > \phi_c$ (the rays $y/n = \phi_c$ are shown in Fig. 9). This particular contour has other configurations for region II if $y/n < \phi_c$ (in this case the w_{sd} segment does not arise), and for the other regions in (54), but they are not displayed here.

This second head wave has a plane surface for a wave front which is given by $t = t_{sdc}$ for $y/n > \phi_c$ and $x/r > c_d/c$. This wave,

referred to as the plane head wave, only exists for $c > c_d$ and then it is generated by the surface intersection of the dilatational wave front at $t = t_{dc}$ and it propagates in front of $t = t_{sc}$, as shown in Fig. 9. For $x/r = c_d/c$ the plane head wave front is tangent to the conical head wave front and for $x/r < c_d/c$ it does not exist because its generator, $t = t_{dc}$, does not exist, as shown in Fig. 5. In the region bounded by $x/r < c_d/c$ and $x/\rho > c_s/c$ the plane head wave ends. This is reflected in u_{zs} by the fact that the last term is discontinuous for $t = t_E$ and the integral in the second term is improper for $t = t_E$. The surface defined by $t = t_E$, which is not shown in any of the figures, is not expected to be a wave front for the same reason as given above for $t = t_B$.

For $c_s < c < c_d$ the plane head wave front does not exist, which can be seen in (55) since now $H((x/r) - (c_d/c)) = 0$. Physically this is expected since its generator, $t = t_{dc}$, does not exist. In this case the last term in u_{zs} still represents an equivoluminal disturbance propagating in front of $t = t_{sc}$. However, now it propagates behind the surface $t = t_E$, which is behind the conical head wave front at $t = t_{sd}$, and which makes the last term indistinguishable as a separate wave. Finally, for $c < c_s$ the last term does not contribute to u_{zs} , which can be seen in (55) since $H((x/r) - (c_d/c)) = 0$ and $H((x/\rho) - (c_s/c)) = 0$.

Total Displacement Field

The total disturbance comprising u_z is the sum of u_{zd} and u_{zs} . Similar expressions can be computed for u_x and u_y , and all three displacements are written as

$$u_j(\underline{x}, t) = \sum_{\beta=1}^6 u_{j\beta}(\underline{x}, t) \quad , \quad (j = x, y, z) \quad (64)$$

for $0 \leq r < \infty$, $0 \leq \theta \leq \pi$ (or $-\infty < x < \infty$, $0 \leq y < \infty$), $0 < z < \infty$, and $0 \leq c < \infty$, where

$$u_{j1}(\underline{x}, t) = H(t-t_d) P \int_0^{T_d} \operatorname{Re} \left[K_{jd}(q_d, w, \theta) \frac{dq_d}{dt} \right] dw \quad , \quad (65)$$

$$u_{j2}(\underline{x}, t) = H(t-t_s) P \int_0^{T_s} \operatorname{Re} \left[K_{js}(q_s, w, \theta) \frac{dq_s}{dt} \right] dw \quad , \quad (66)$$

$$u_{j3}(\underline{x}, t) = H(t-t_{sd}) H(t_B - t) H\left(\frac{r}{\rho} - \frac{c_s}{c_d}\right) P \int_{A_{sd}}^{T_{sd}} \operatorname{Re} \left[K_{js}(q_{sd}, w, \theta) \frac{dq_{sd}}{dt} \right] dw \quad , \quad (67)$$

$$u_{j4}(\underline{x}, t) = \operatorname{Re} \left[\hat{K}_{jd}(w_d, \theta) \frac{dw_d}{dt} \right] H(t-t_{dc}) H(t-t_L) H(x) \quad , \quad (68)$$

$$u_{j5}(\underline{x}, t) = \operatorname{Re} \left[\hat{K}_{js}(w_s, \theta) \frac{dw_s}{dt} \right] H(t-t_{sc}) H(t-t_L) H(x) \quad , \quad (69)$$

$$u_{j6}(\underline{x}, t) = \operatorname{Re} \left[\hat{K}_{js}(w_{sd}, \theta) \frac{dw_{sd}}{dt} \right] H\left(\frac{y}{n} - \phi_c\right) \left[H(t-t_{sdc}) H\left(\frac{x}{r} - \frac{c_d}{c}\right) \right. \\ \left. + H(t-t_E) H\left(\frac{x}{\rho} - \frac{c_s}{c}\right) H\left(\frac{c_d}{c} - \frac{x}{r}\right) - H(t-t_{sc}) H\left(\frac{x}{\rho} - \frac{c_s}{c}\right) \right] H(x) \quad . \quad (70)$$

The symbols which have not been previously defined are

$$\hat{K}_{xd}(w, \theta) = \frac{\gamma \sec \theta}{\pi c \mu R} m_o \bigg|_{q = Q_c^+} \quad , \quad (71)$$

$$\hat{K}_{xs}(w, \theta) = \frac{-2\gamma \sec \theta}{\pi c \mu R} m_d m_s \bigg|_{q = Q_c^+} \quad , \quad (72)$$

$$\hat{K}_{yd}(w, \theta) = \frac{\sec^2 \theta}{\pi c \mu R} (\gamma \sin \theta - iw) m_o \bigg|_{q = Q_c^+} \quad , \quad (73)$$

$$\hat{K}_{ys}(w, \theta) = \frac{-2 \sec^2 \theta}{\pi c \mu R} (\gamma \sin \theta - iw) m_d m_s \Big|_{q = Q_c^+} \quad (74)$$

In this form the first three terms in u_j represent a system of waves which emanate from the initial position of the load as if they were generated by a stationary point source. On the other hand, the last three terms represent disturbances that trail behind the load and whose wave geometry depends on the speed of the load relative to the body wave speeds.

Finally, it is noted that the interior displacements given here are not uniformly valid in z , as $z \rightarrow 0$, because the particular contours in the q - and w -planes wrap around the poles at $q = Q_R^+$ and $w = S_R^+$ as $z \rightarrow 0$. Therefore, to obtain the surface displacements it is necessary to return to the formal solution in (7) and (8), set $z = 0$, and then invert the displacements (or equivalently, evaluate the contribution of the poles at $q = Q_R^+$ and $w = S_R^+$ as $z \rightarrow 0$, and combine the results with the interior displacements in (64) - (70) evaluated for $z = 0$). However, since Payton [1] and Lansing [2] have already investigated the surface displacements, they are not displayed here; but they are given in [13] in context with the technique used here.

5. WAVE FRONT EXPANSIONS

The wave form of the solution given in (64) - (70) is advantageous for evaluating the displacements near the wave fronts. To facilitate these expansions for the waves emanating from the initial position of the load, the time dependence in the limits of the integrals in (65) - (70) is removed by the transformation

$$w = [A^2 + (B^2 - A^2)\sin^2\alpha]^{\frac{1}{2}}, \quad (75)$$

where A is the lower limit and B is the upper limit of the particular integral in question, and the α range of integration is 0 to $\pi/2$. Furthermore, this transformation removes a half-order singularity in the integrand of u_{j1} and u_{j2} which is introduced by the differentials of q_d and q_s . Then u_{j1} , u_{j2} , and u_{j3} are evaluated as $t \rightarrow t_d$, $t \rightarrow t_s$, and $t \rightarrow t_{sd}$, respectively, by first expanding the appropriate integrands and then integrating these expansions from 0 to $\pi/2$. Special attention must be given to u_{j3} since the integral in this term is improper for $t = t_s$. This term is evaluated by first approximating the improper integral for t near t_s and then letting $t \rightarrow t_s$. In this way one finds

$$u_{j1} = A_{j1} + O(t - t_d) \quad \text{as } t \rightarrow t_d, \quad (76)$$

$$u_{j2} = \begin{cases} A_{j2} + O(t - t_s) & \text{for } \frac{r}{\rho} < \frac{c_s}{c_d} \\ A'_{j2} + O\left((t - t_s)^{\frac{1}{2}}\right) & \text{for } \frac{r}{\rho} > \frac{c_s}{c_d} \end{cases} \quad \text{as } t \rightarrow t_s, \quad (77)$$

$$u_{j3} = A_{j3}(t - t_{sd}) + O\left((t - t_{sd})^2\right) \quad \text{as } t \rightarrow t_{sd} \quad \text{for } \frac{r}{\rho} > \frac{c_s}{c_d}, \quad (78)$$

$$u_{j3} = A'_{j3} \log \left(\left| \frac{t}{t_s} - 1 \right| \right) + O(1) \quad \text{as } t \rightarrow t_s \quad \text{for } \frac{r}{\rho} > \frac{c_s}{c_d}, \quad (79)$$

for $j = x, y, z$, where the wave front coefficients are given in the appendix. These expansions are valid for $0 \leq \theta \leq \pi$, $z > 0$, and $0 \leq c < \infty$, except that (76) is not valid along the rays $x/\rho = c_d/c$ since A_{ji} is unbounded along these rays. Similarly, (77) and (79) are not valid along $x/\rho = c_s/c$, and (78) is not valid along $x/r = c_d/c$.

As the expansions in (76) - (78) show, u_j has a step discontinuity

across the hemispherical wave fronts at $t = t_d$ and $t = t_s$, and it is continuous through $t = t_{sd}$. However, for $r/\rho > c_s/c_d$ the disturbance near $t = t_s$ is dominated by the logarithmic singularity shown in (79). This singularity is two-sided in that u_j becomes unbounded as $t \rightarrow t_s$ for $t < t_s$ and for $t > t_s$, and it is symmetric about $t = t_s$.

Since the waves trailing behind the load are in an algebraic form, they are expanded algebraically near their wave fronts, yielding

$$u_{j4} = A_{j4}(t - t_{dc})^{-\frac{1}{2}} + O\left((t - t_{dc})^{\frac{1}{2}}\right) \quad \text{as } t \rightarrow t_{dc}, \quad (80)$$

$$u_{j5} = \begin{cases} A_{j5}(t - t_{sc})^{-\frac{1}{2}} + O\left((t - t_{sc})^{\frac{1}{2}}\right) & \text{for } \frac{y}{n} < \phi_c \\ A'_{j5}(t - t_{sc})^{-\frac{1}{2}} + O(1) & \text{for } \frac{y}{n} > \phi_c \end{cases} \quad \text{as } t \rightarrow t_{sc}, \quad (81)$$

$$u_{j6} = A_{j6}(t - t_{sdc})^{\frac{1}{2}} + O\left((t - t_{sdc})^{3/2}\right) \quad \text{as } t \rightarrow t_{sdc} \text{ for } \frac{y}{n} > \phi_c, \quad (82)$$

$$u_{j6} = A'_{j6}(t_{sc} - t)^{-\frac{1}{2}} + O(1) \quad \text{as } t \rightarrow t_{sc} \text{ for } \frac{y}{n} > \phi_c, \quad (83)$$

for $j = x, y, z$. These expansions are valid for $0 \leq \theta \leq \pi$ and $z > 0$, except that (80) only arises for $c > c_d$ and $x/\rho \geq c_d/c$, the upper one in (81) for $c > c_d$ and $x/\rho \geq c_s/c$, the lower one in (81) and (83) for $c > c_s$ and $x/\rho \geq c_s/c$, and (82) for $c > c_d$ and $x/r \geq c_d/c$. These latter conditions correspond to when and where the wave fronts $t = t_{dc}$, $t = t_{sc}$, and $t = t_{sdc}$ arise in the half-space.

As (80) and (81) show, u_j has a half-order singularity behind the conical wave fronts at $t = t_{dc}$ and $t = t_{sc}$. In addition, u_j contains a half-order singularity in front of $t = t_{sc}$, as (83) shows, producing another two-sided singularity in u_j . If $c > c_d$, this two-sided singularity exists across $t = t_{sc}$ for $y/n > \phi_c$; if $c_s < c < c_d$, it exists across the entire conical wave front at $t = t_{sc}$; and if $c < c_s$,

it does not exist at all. Also, u_j is continuous through the head wave front at $t = t_{sdc}$, as it is through $t = t_{sd}$. Finally, it should be noted that the disturbance near the wave fronts trailing behind the load is a half-order stronger than near the corresponding (compare wave fronts involving the same type of disturbance) wave fronts emanating from the initial position of the load. This can be seen, for example, by comparing the wave front expansions of u_{j1} as $t \rightarrow t_d$ and u_{j4} as $t \rightarrow t_{dc}$.

6. STATIONARY POINT LOAD

A special case of the moving load problem is that of a half-space whose surface is excited by a stationary point load with step time dependence. A solution to this problem, which was first worked on by Lamb [14], is obtained here by letting $c \rightarrow 0$ in (64) - (70) and expressing the displacements in their cylindrical components, to give

$$u_{\sigma}(\underline{x}, t) = \sum_{\beta=1}^3 u_{\sigma\beta}(\underline{x}, t) \quad , \quad (\sigma = r, z) \quad , \quad (84)$$

$$u_{\theta}(\underline{x}, t) = 0 \quad , \quad (85)$$

for $0 \leq r < \infty$, $0 \leq \theta \leq \pi$, and $0 < z < \infty$, where

$$u_{\sigma 1}(\underline{x}, t) = H(t-t_d) \int_0^{T_d} \operatorname{Re} \left[K_{\sigma d}^0(q_d, w) \frac{dq_d}{dt} \right] dw \quad , \quad (86)$$

$$u_{\sigma 2}(\underline{x}, t) = H(t-t_s) \int_0^{T_s} \operatorname{Re} \left[K_{\sigma s}^0(q_s, w) \frac{dq_s}{dt} \right] dw \quad , \quad (87)$$

$$u_{\sigma 3}(\underline{x}, t) = H(t-t_{sd}) H(t_B - t) H\left(\frac{r}{\rho} - \frac{c_s}{c_d}\right) \int_{A_{sd}}^{T_{sd}} \operatorname{Re} \left[K_{\sigma s}^0(q_{sd}, w) \frac{dq_{sd}}{dt} \right] dw, \quad (88)$$

in which

$$\left. \begin{aligned} K_{rd}^O(q, w) &= -iqm_O M, & K_{rs}^O(q, w) &= 2iqm_d m_s M \\ K_{zd}^O(q, w) &= m_d m_O M, & K_{zs}^O(q, w) &= -2m_d (q^2 + w^2) M \end{aligned} \right\} \quad (89)$$

$$M = \frac{1}{\pi^2 c_d^{\mu} R} \quad . \quad (90)$$

The wave geometry associated with these displacements is the same as for $c < c_s$, as shown in Figs. 6b and 8b, except that the contours $t = t_L$ and $t = t_{sdc}^O$ are not present in the $c = 0$ solution.

It should be noted that Eason [15], and Cinelli and Fugelso [16] have also worked on Lamb's point load problem for the interior of the half-space using transforms. Their results are also in the form of single integrals, but they do not readily display the wave fronts associated with a concentrated surface load. Mitra [11] has derived the interior displacements for a half-space whose surface is excited by a uniform disk of pressure. He used Cagniard's technique and DeHoop's transformation, but his solution technique is adapted to the axisymmetry of his problem. Furthermore, he mentions that his solution technique is applicable to Lamb's point load problem, but he gives no results. Also, Pekeris [17] has thoroughly analyzed the surface displacements due to a stationary point load. His results agree in detail with those given here if the latter are extended to include $z = 0$. Finally, Lang [18,19] and Craggs [20] have also worked on Lamb's problem, but they did not use transforms.

Wave front expansions which correspond to a stationary point load can be computed from the integrals in (86) - (88), or they can be obtained from the expansions in Section 5. In fact, these expansions

have the same form as those given for u_{j1} , u_{j2} , and u_{j3} in (76) - (79); the only difference is that the coefficients A_{j1} , A_{j2} , A'_{j2} , A_{j3} , and A'_{j3} must be evaluated for $c = 0$. The wave front expansions for a stationary point load were also computed by Knopoff and Gilbert [21]. They used a Tauberian theorem and the saddle point technique to evaluate a formal transform solution near the wave fronts. Their results agree in detail with those that are obtained here, except that they did not detect the logarithmic singularity at $t = t_s$ for $r/\rho > c_s/c_d$, as first noted by Aggarwal and Ablow [22].

7. STEADY-STATE RESPONSE

By algebraic manipulations it can be shown that u_{j4} , u_{j5} , and u_{j6} in (68) - (70), less $H(x)$ and $H(t - t_L)$, are only functions of the coordinates ξ, y, z which are invariant to the translation of the load (see [13] for details). Therefore, these terms are constant at a fixed position in a coordinate system moving with the load. For $c > c_d$ and long time ($t \rightarrow \infty$), $H(t - t_L) = 1$ and $H(x) = 1$ for points near the load, and the load "runs away" from the waves emanating from the initial position of the load. Consequently, for $c > c_d$ the waves trailing behind the load represent the steady-state displacement field (i.e., $u_j = u_{j4} + u_{j5} + u_{j6}$ as $t \rightarrow \infty$ for $c > c_d$ and points near the position of the load, $j = x, y, z$). The wave geometry corresponding to these steady-state displacements is shown in Fig. 9, where only the waves that trail behind the load are shown.

Lansing [3] has also computed the steady-state displacements due to a moving point load. He used a technique which assumed steady-stateness from the outset and his results are in the form of single

integrals. As a special case, in the plane under the path of the load ($y = 0$ plane), and for $\lambda = \mu$ and $c > c_d$, Lansing integrated his results, leaving the displacements in an algebraic form which agrees with that one obtained here.

Finally, for $c < c_d$ the waves trailing behind the load do not represent the entire steady-state displacement field. In this case the waves emanating from the initial position of the load also contribute and they must be evaluated for $t \rightarrow \infty$.

REFERENCES

1. Payton, R. G., "An Application of the Dynamic Betti-Rayleigh Reciprocal Theorem to Moving-Point Loads in Elastic Media," *Quart. Appl. Math.*, Vol. 21, 1964, pp. 299-313.
2. Lansing, D. L., "The Displacements in an Elastic Half-Space Due to a Moving Concentrated Normal Load," *NASA Technical Report, NASA TR R-238*, 1966.
3. Mandel, J. and Avramesco, A., "Déplacements Produits par une Charge Mobile à la Surface d'un Semi-Espace Elastique," *Compt. Rend. Acad. Sci.*, Paris, Vol. 252, pt. 3, 1961, pp. 3730-3735.
4. Papadopoulos, M., "The Elastodynamics of Moving Loads," *J. Austral. Math. Soc.*, Vol. 3, 1963, pp. 79-92.
5. Grimes, C. K., "Studies on the Propagation of Elastic Waves in Solid Media," *Ph.D. Thesis*, California Institute of Technology, Pasadena, California, 1964.
6. Eason, G., "The Stresses Produced in a Semi-Infinite Solid by a Moving Surface Force," *Int. J. Engng. Sci.*, Vol. 2, 1965, pp. 581-609.
7. Chao, C. C., "Dynamic Response of an Elastic Half-Space to Tangential Surface Loadings," *J. Appl. Mech.*, Vol. 27, 1960, pp. 559-567.
8. Scott, R. A. and Miklowitz, J., "Transient Non-Axisymmetric Wave Propagation in an Infinite Isotropic Elastic Plate," in press, *Int. J. Solids and Structures*.
9. Cagniard, L., Reflection and Refraction of Progressive Seismic Waves, Translated by E. A. Flinn and C. H. Dix, McGraw-Hill Book Co., New York, 1962.
10. DeHoop, A. T., "A Modification of Cagniard's Method for Solving Seismic Pulse Problems," *Appl. Sci. Res.*, Section B, Vol. 8, 1959, pp. 349-356.
11. Mitra, M., "Disturbance Produced in an Elastic Half-Space by Impulsive Normal Pressure," *Proc. Camb. Phil. Soc.*, Vol. 60, 1964, pp. 683-696.
12. Carslaw, H. S. and Jaeger, J. C., Operational Methods in Applied Mathematics, Oxford University Press, 1941.
13. Gakenheimer, D. C., "Transient Excitation of an Elastic Half-Space By a Point Load Traveling on the Surface," *Ph.D. Thesis*, California Institute of Technology, Pasadena, California, 1968.

14. Lamb, H., "On the Propagation of Tremors Over the Surface of an Elastic Solid," Phil. Trans. Roy. Soc. Lond. (A), Vol. 203, 1904, pp. 1-42.
15. Eason, G., "The Displacements Produced in an Elastic Half-Space by a Suddenly Applied Surface Force," J. Inst. Maths Applics, Vol. 2, 1966, pp. 299-326.
16. Cinelli, G. and Fugelso, L. E., "Theoretical Study of Ground Motion Produced by Nuclear Blasts," Mech. Res. Div. American Machine and Foundry Company, Report under Contract AF 29(601)-1190 with AF SWC, 1959.
17. Pekeris, C. L., "The Seismic Surface Pulse," Proc. Nat. Acad. Sci., Vol. 14, 1955, pp. 469-480.
18. Lang, H. A., "The Complete Solution for an Elastic Half-Space Under a Point Step Load," Rep. No. P-1141, Rand Corp., Santa Monica, California, 1957.
19. Lang, H. A., "Surface Displacements in an Elastic Half-Space," ZAMM, Vol. 41, 1961, pp. 141-153.
20. Craggs, J. W., "On Axially Symmetric Waves, III. Elastic Waves in a Half-Space," Proc. Cambridge Philos. Soc., Vol. 59, 1963, pp. 803-809.
21. Knopoff, L. and Gilbert, F., "First Motion Methods in Theoretical Seismology," J. Acoust. Soc. Amer. Vol. 31, 1959, pp. 1161-1168.
22. Aggarwal, H. R. and Ablow, C. M., "Solution to a Class of Three-Dimensional Pulse Propagation Problems in an Elastic Half-Space," Int. J. Engng Sci., Vol. 5, 1967, pp. 663-679.

APPENDIX

Wave Front Coefficients

The wave front coefficients are written in one expression for all three displacements like the components of a vector.

$$(A_{x1}, A_{y1}, A_{z1}) = (x, y, z) \frac{(z/2\pi\mu\rho)a_1}{a_3(a_1^2 + 4r^2za_2)} \quad (91)$$

$$(A_{x2}, A_{y2}, A_{z2}) = (-xz, -yz, r^2) \frac{(z/\pi\mu\rho)a_4}{a_6(a_5^2 + 4r^2za_4)} \quad (92)$$

$$(A'_{x2}, A'_{y2}, A'_{z2}) = (-xz, -yz, r^2) \frac{(4r^2z^2/\pi\mu\rho)a_7^2}{a_6(a_5^4 + 16r^4z^2a_7^2)} \quad (93)$$

$$(A_{x3}, A_{y3}, A_{z3}) = (xe_1, ye_1, -r) \frac{(c_d/\pi\mu r^{3/2})e_1^{3/2}}{e_2^2a_8a_9} \quad (94)$$

$$(A'_{x3}, A'_{y3}, A'_{z3}) = (-xz, -yz, r^2) \frac{(z/\pi^2\mu\rho)a_7a_5^2}{a_6(a_5^4 + 16r^4z^2a_7^2)} \quad (95)$$

$$(A_{x4}, A_{y4}, A_{z4}) = (n, yM_d, zM_d) \frac{(z/\pi\mu)M_d^{\frac{1}{2}}b_1}{(2cn)^{\frac{1}{2}}(b_1^2 + 4zM_db_2b_3)} \quad (96)$$

$$(A_{x5}, A_{y5}, A_{z5}) = (-nzM_s, -yzM_s^2, b_6) \frac{(2z/\pi\mu)M_s^{\frac{1}{2}}b_5}{(2cn)^{\frac{1}{2}}(b_4^2 + 4zM_sb_5b_6)} \quad (97)$$

$$(A'_{x5}, A'_{y5}, A'_{z5}) = (-nzM_s, -yzM_s^2, b_6) \frac{(8z^2/\pi\mu)M_s^{3/2}b_6b_7^2}{(2cn)^{\frac{1}{2}}(b_4^4 + 16z^2M_s^2b_6^2b_7^2)} \quad (98)$$

$$(A_{x6}, A_{y6}, A_{z6}) = (\gamma e_1, \gamma e_1 M_d, -1) \frac{2(2c_d)^{\frac{1}{2}}e_1^{3/2}M_d}{\pi\mu e_2^2b_8^3} \quad (99)$$

$$(A'_{x6}, A'_{y6}, A'_{z6}) = (nzM_s, yzM_s^2, -b_6) \frac{(2z/\pi\mu)M_s^{\frac{1}{2}}b_4^2b_7}{(2cn)^{\frac{1}{2}}(b_4^4 + 16z^2M_s^2b_6^2b_7^2)} \quad (100)$$

in which

$$\begin{aligned}
 a_1 &= (\ell^2 \rho^2 - 2r^2) \quad , \quad a_5 = (\rho^2 - 2r^2) \\
 a_2 &= (\ell^2 \rho^2 - r^2)^{\frac{1}{2}} \quad , \quad a_6 = \left(1 - \frac{cx}{c_s \rho}\right) \\
 a_3 &= \left(1 - \frac{cx}{c_d \rho}\right) \quad , \quad a_7 = (r^2 - \ell^{-2} \rho^2)^{\frac{1}{2}} \\
 a_4 &= (\ell^{-2} \rho^2 - r^2)^{\frac{1}{2}} \quad , \quad a_8 = (re_1 - z)^{\frac{1}{2}} \\
 a_9 &= \left(1 - \frac{cx}{c_d r}\right)
 \end{aligned} \tag{101}$$

$$\begin{aligned}
 b_1 &= [n^2(M_s^2 - 1) - 2y^2 M_d^2] \quad , \quad b_5 = (z^2 M_s^2 - n^2 M_{sd}^2)^{\frac{1}{2}} \\
 b_2 &= (z^2 M_d^2 + n^2 M_{sd}^2)^{\frac{1}{2}} \quad , \quad b_6 = (y^2 M_s^2 + n^2) \\
 b_3 &= (y^2 M_d^2 + n^2) \quad , \quad b_7 = (n^2 M_{sd}^2 - z^2 M_s^2)^{\frac{1}{2}} \\
 b_4 &= [n^2(M_s^2 - 1) - 2y^2 M_s^2] \quad , \quad b_8 = (y M_{sd} - z M_d)^{\frac{1}{2}}
 \end{aligned} \tag{102}$$

$$e_1 = (\ell^2 - 1)^{\frac{1}{2}} \quad , \quad e_2 = (\ell^2 - 2) \tag{103}$$

$$M_d = \left(\frac{c^2}{c_d^2} - 1\right)^{\frac{1}{2}} \quad , \quad M_s = \left(\frac{c^2}{c_s^2} - 1\right)^{\frac{1}{2}} \quad , \quad M_{sd} = \left(\frac{c^2}{c_s^2} - \frac{c^2}{c_d^2}\right)^{\frac{1}{2}} \tag{104}$$

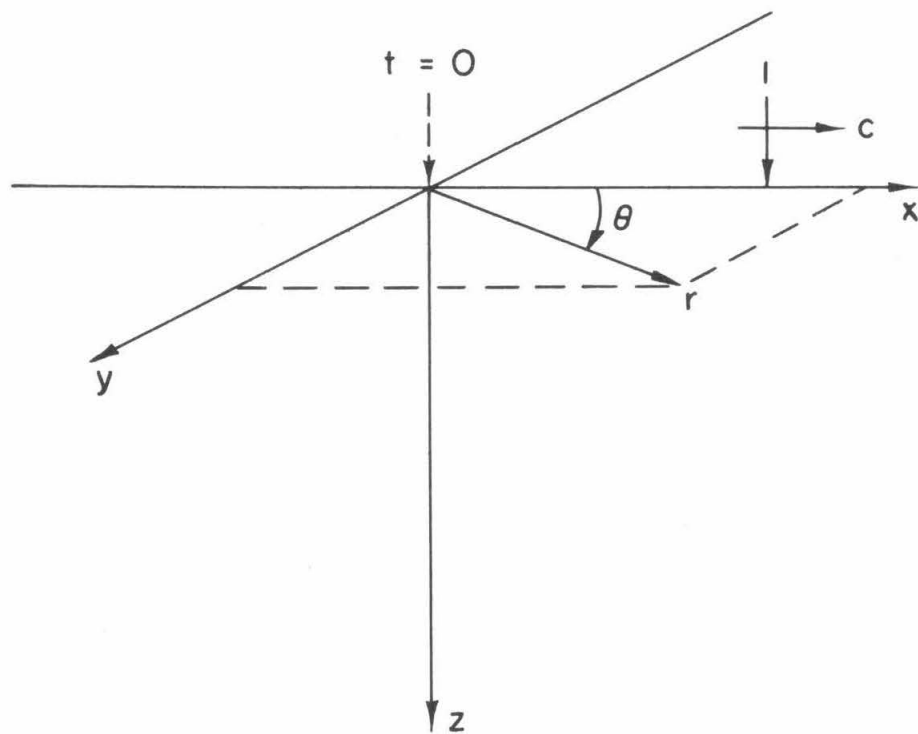


FIGURE 1
Traveling Point Load Problem

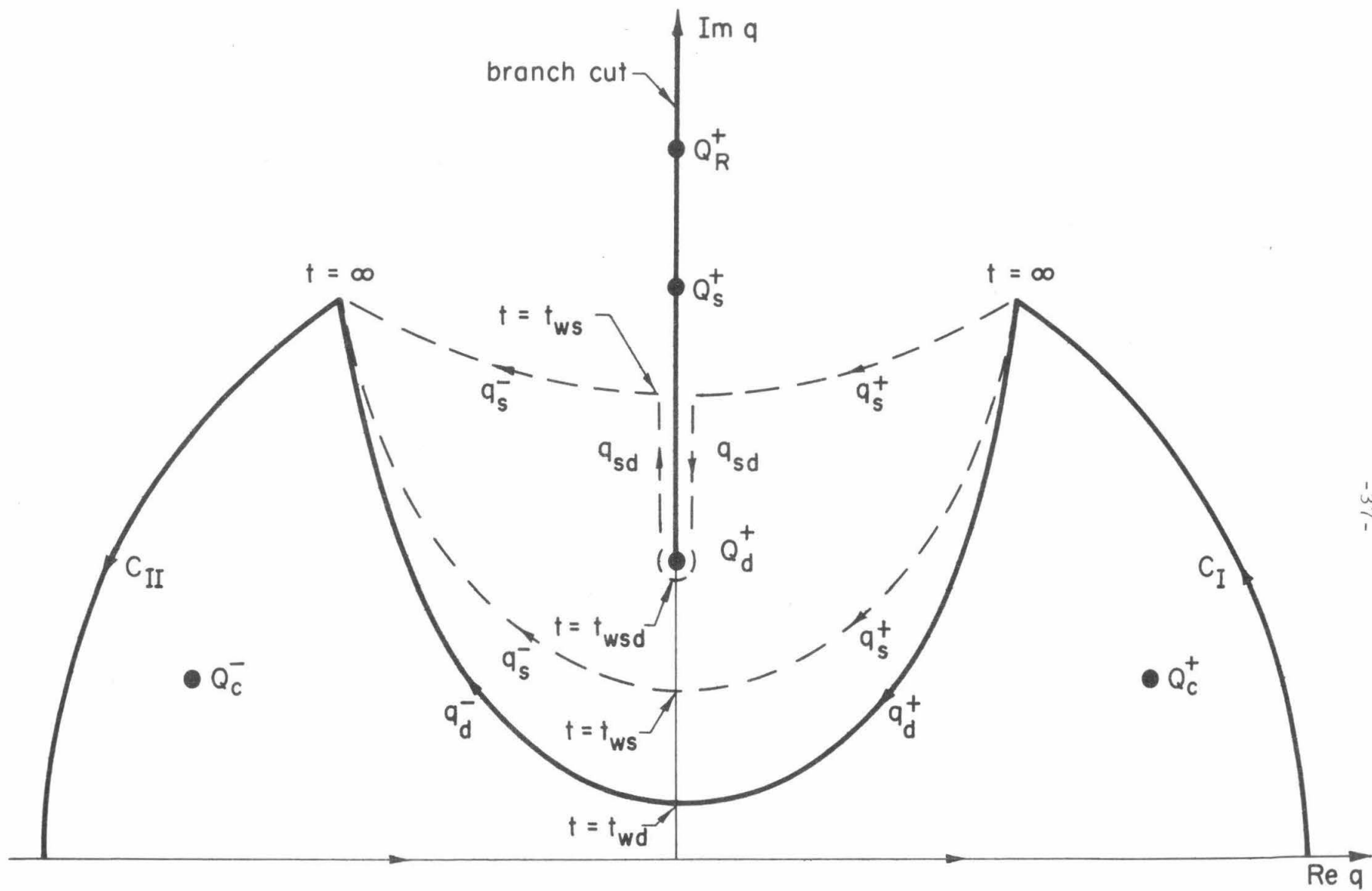


FIGURE 2

Contour Integration in the q -Plane

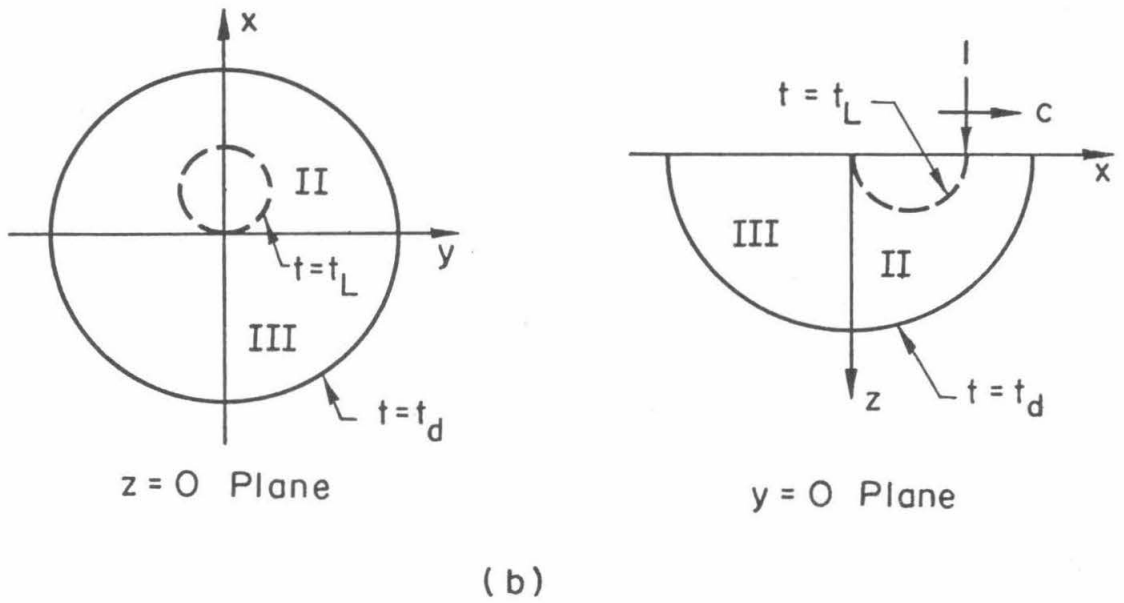
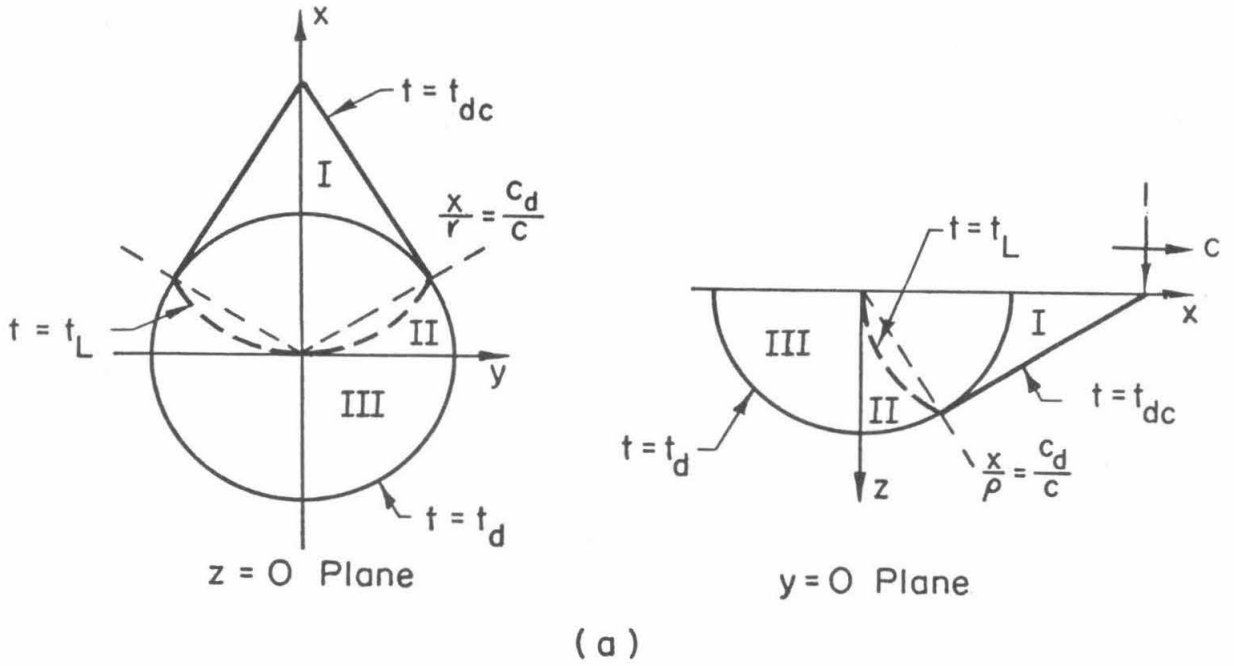


FIGURE 3
Dilatational Wave Pattern for (a) Supersonic Load Motion and
(b) Transonic and Subsonic Load Motion

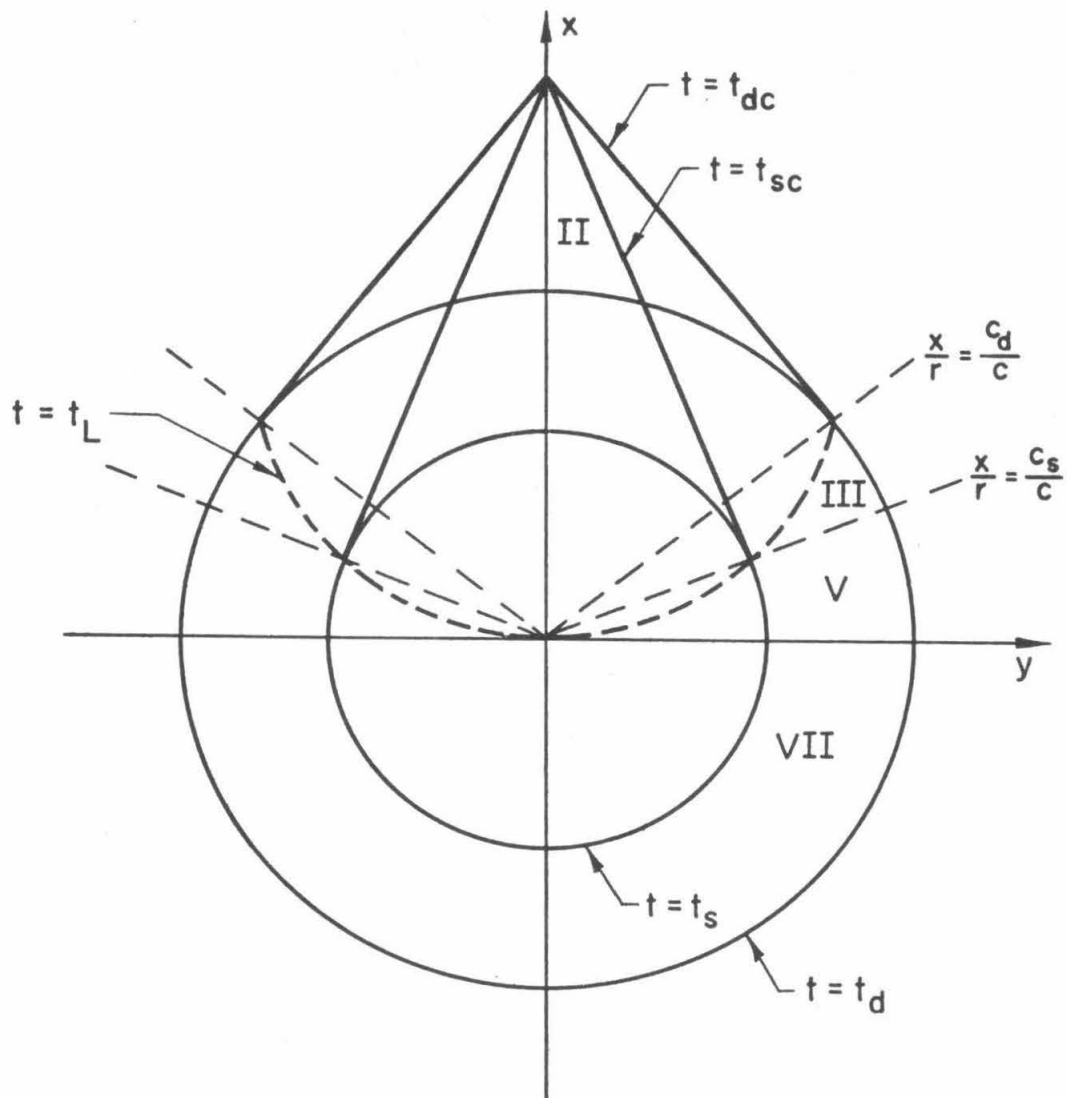


FIGURE 5
Wave Pattern in the Surface Plane
for Supersonic Load Motion

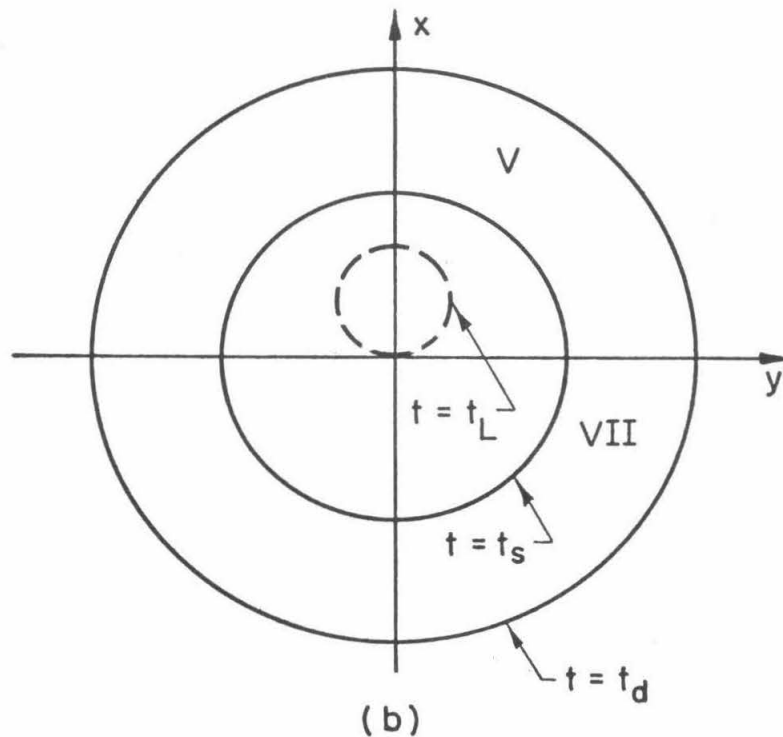
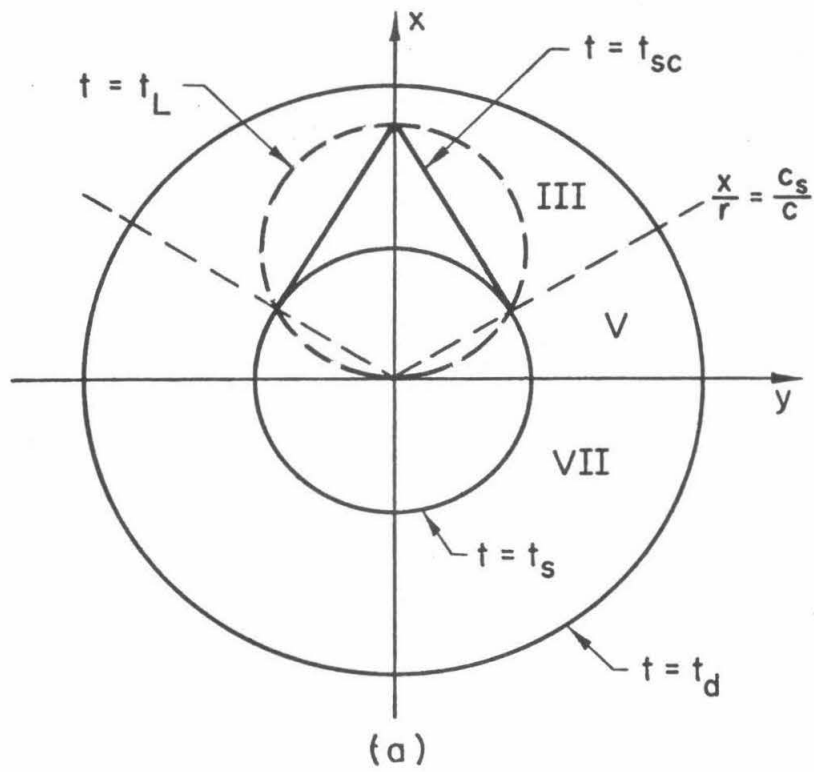


FIGURE 6

Wave Pattern in the Surface Plane for (a) Transonic Load Motion and
(b) Subsonic Load Motion

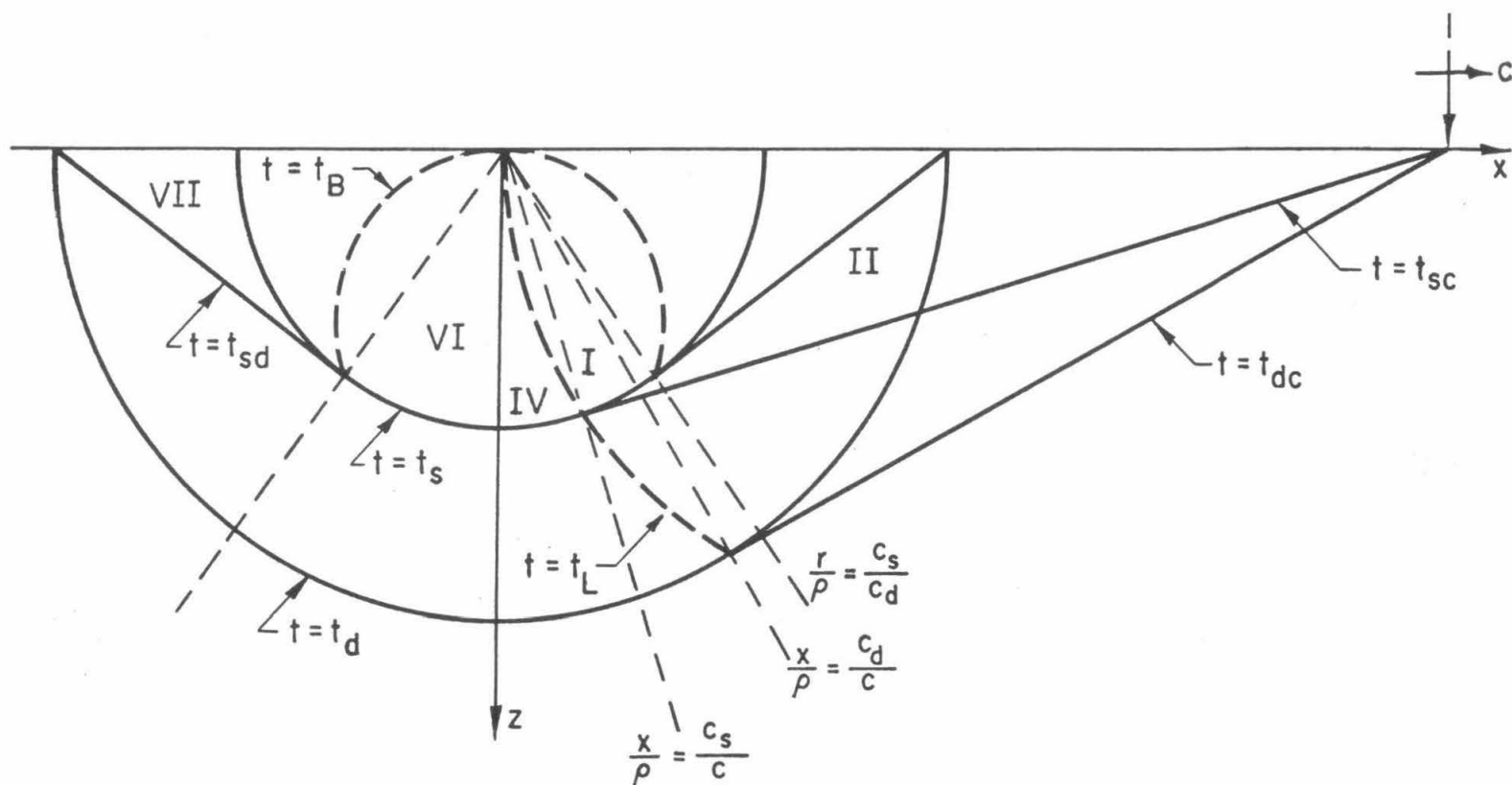


FIGURE 7

Wave Pattern in the Plane Under the Path of the Load for
Supersonic Load Motion

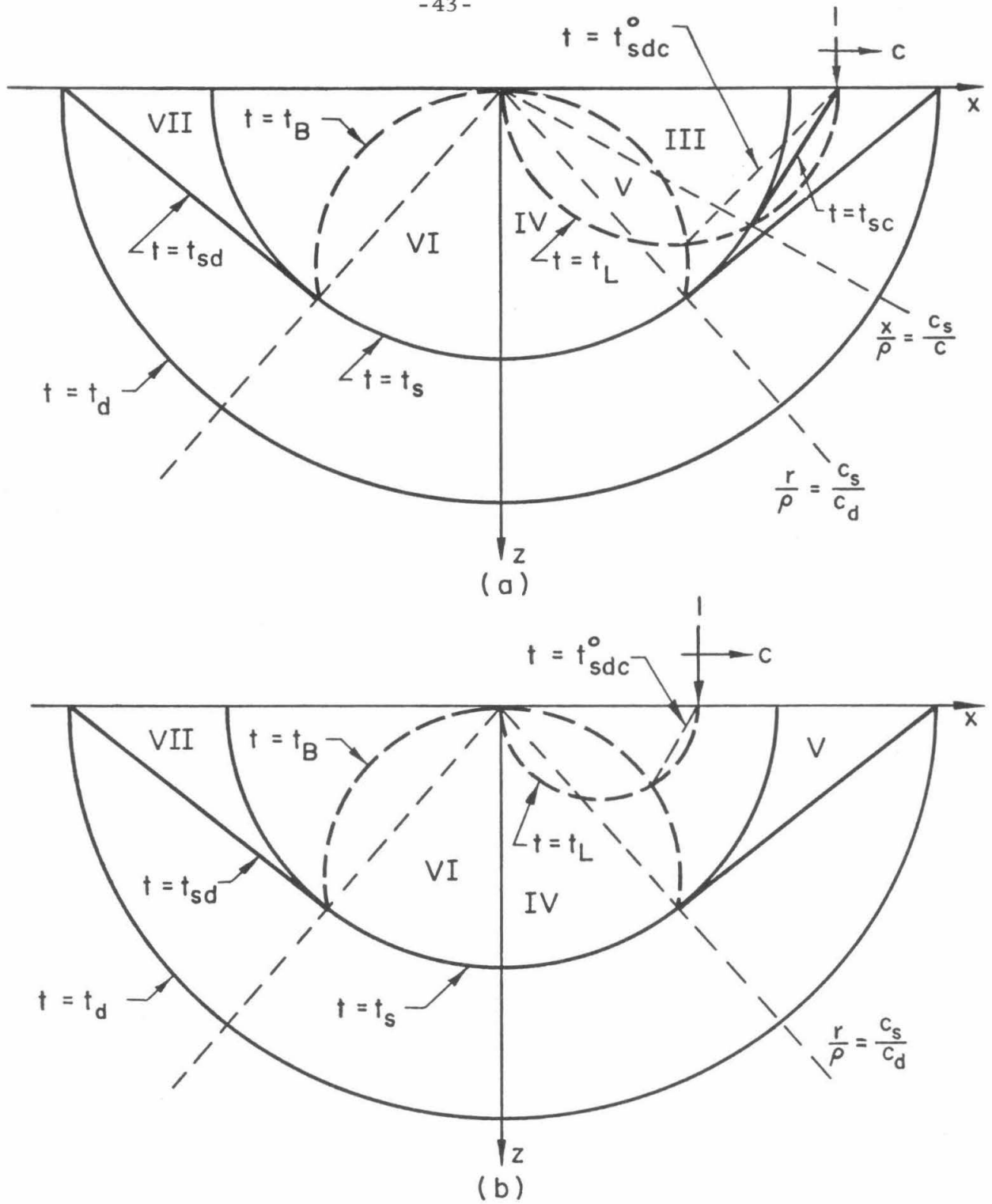


FIGURE 8

Wave Pattern in the Plane Under the Path of the Load for
(a) Transonic Load Motion and (b) Subsonic Load Motion

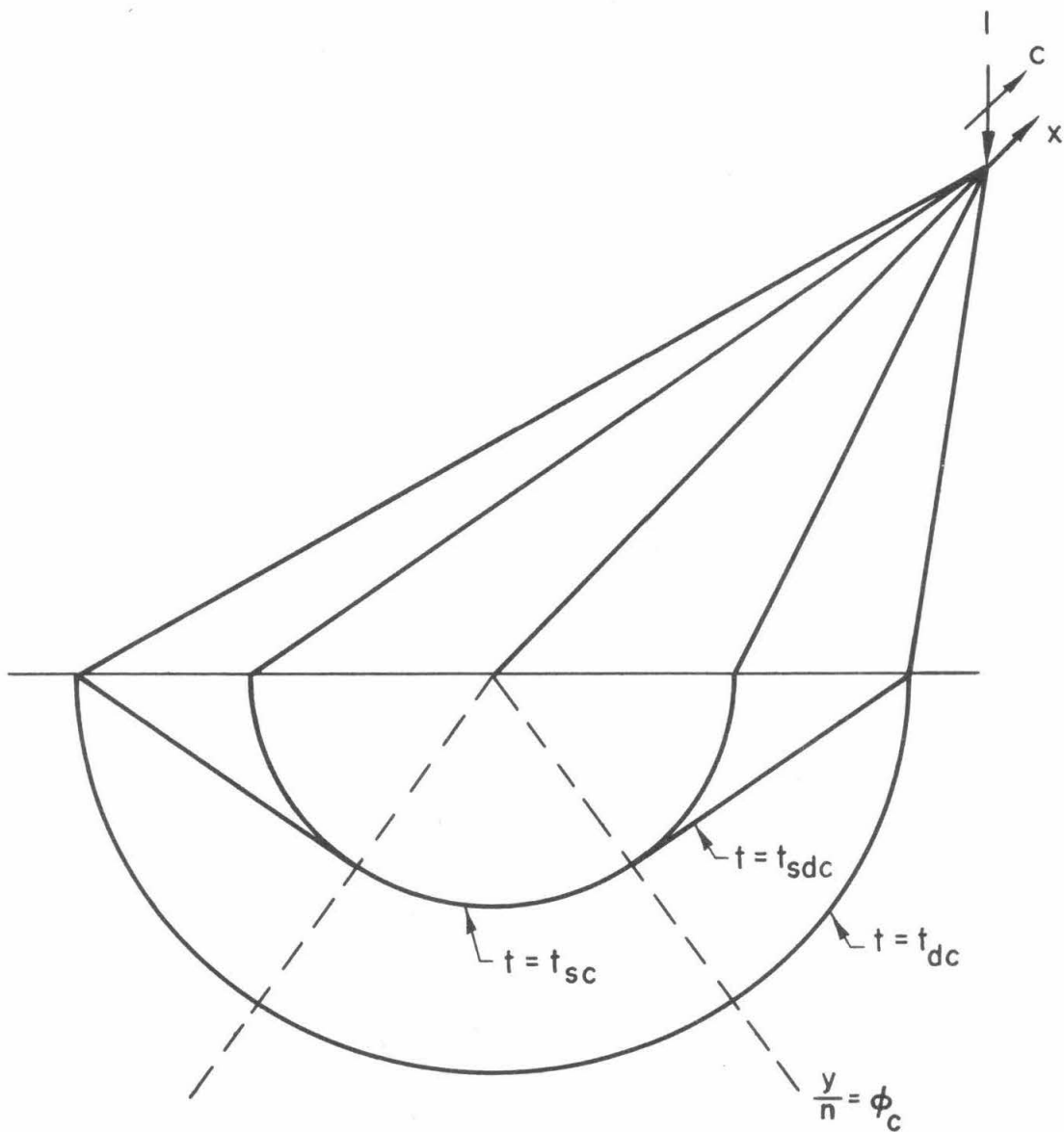


FIGURE 9

Waves Trailing Behind the Load for
Supersonic Load Motion

ACKNOWLEDGMENT

The first author is indebted to the National Aeronautics and Space Administration for the support of a Graduate Traineeship.